This article is part of the

Proceedings of the 16th Minisymposium Verfahrenstechnik and 7th Partikelforum (TU Wien, Sept. 21/22, 2020)

Title:
Statistical Modeling of the Coating Uniformity in a Wurster Coating Process

Corresponding author:
Stefan Madlmeir (RCPE GmbH), stefan.madlmeir@rcpe.at

Date of submission:
22.07.20

Date of revision:
10.09.20

Date of acceptance:
10.09.20

Chapter ID:
DiV5-(04)

Length:
5 pages

ISBN (full book):
978-3-903337-01-5

Statistical Modeling of the Coating Uniformity in a Wurster Coating Process

Stefan Madlmeir[1], **Stefan Radl**[2]
1: RCPE GmbH, Graz, Austria, stefan.madlmeir@rcpe.at
2: Institute of Process and Particle Engineering, Graz University of Technology, Graz, Austria

Keywords: Pharmaceutical coating, Wurster coating process, CFD-DEM, statistical modeling, coating uniformity

Abstract

Modeling pharmaceutical coating processes involves considering many complex phenomena. Detailed models fail to cover the whole coating duration due to the large computational expense, while the input parameters for statistical models are usually difficult to obtain. In the present work a statistical model was derived from detailed numerical simulations of a Wurster coater. The model provides the possibility to evaluate the impact of the inlet air flow rate, spray rate, coating level and solid mass fraction in the spray solution on the coating uniformity over the full process duration. It was found that the coating uniformity scales with the inverse square root of the number of cycles, which the particles undergo during the coating process. Based on the model, a strategy for the systematic optimization of the process parameters is presented.

Introduction

In food and pharmaceutical industry, particle coating is a common unit operation to modify taste, odor or appearance of the product. In addition, the release behavior of drugs can be controlled with so-called functional coatings. To apply the coating layer, a solid coating substance is usually dissolved or dispersed in a liquid and then sprayed onto the particle surface. While the liquid evaporates into the surrounding air, the solid substance remains on the particle. In terms of product quality, small inter- and intra-particle variations of the layer thickness are desired. Amongst others, fluidized bed coating is commonly used for this purpose: the comparably fast mixing in fluidized beds leads to a homogeneous coating layer, and high heat and mass transfer rates are beneficial for evaporating the liquid. Based on the position of the spray nozzle, fluidized bed coaters are divided in (i) top spray coaters, (ii) bottom spray coaters, (iii) Wurster coaters (bottom spray including a draft tube) and (iv) rotary fluid bed coaters [1].

The Wurster coater is a modified bottom spray fluidized bed coating device, containing one cylindrical draft tube (the so called Wurster tube) for every spray nozzle (Figure 1). The particles enter the Wurster tube at the bottom of the container, are sprayed inside the tube and leave it on top. After getting sprayed and when falling back down outside of the tube, the particles are dried. A distributor plate at the air inlet ensures a high fluid volume flow inside the Wurster tube, while the volume flow outside the tube is considerably lower. The higher air flow inside the tube induces the circulation of the particles. The controlled particle movement leads to a high quality coating. Compared with top spray devices the spray-particle contact occurs closer to the nozzle, reducing the loss of coating material due to spray evaporation [2].

The models of the Wurster coating process can be divided into two main groups: (i) statistical models and (ii) mechanistic numerical simulations. Statistical models are usually fast and rather simple, but it is difficult to obtain the realistic input parameters experimentally. Numerical simulations aim for modeling the underlying physical phenomena, and hence are more sophisticated. However, due the computational costs, only a short time period of the whole process can be simulated typically. Although combinations of mechanistic and statistical models exist, a time consuming simulation is still required for each set of process parameter to be investigated [3]–[5].

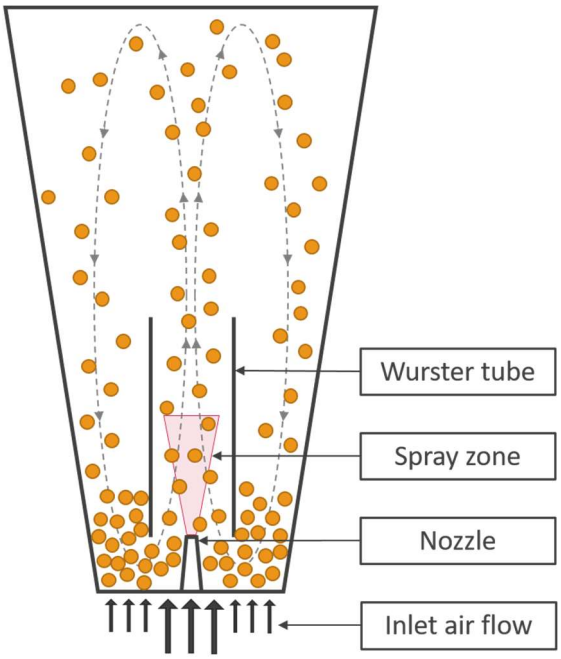

Figure 1: Schematic illustration of the Wurster coating process. The particles pass the spray zone while travelling upwards through the Wurster tube. Subsequently, they are dried during the downwards movement outside of the tube.

In the present study, simulations based on the Computational Fluid Dynamics – Discrete Element Method (CFD-DEM) are used to distill a statistical model for predicting the inter-particle coating uniformity over industrially-relevant process durations. With the resulting model it is possible to vary the inlet air flow rate, spray rate, coating level and the solid mass fraction in the spray solution without the need of new CFD-DEM simulations.

Methods

To determine the particle motion inside the Wurster coater, an Euler-Lagrange approach is used. The applied four-way-coupling includes momentum transfer from the particles to the fluid (i.e., process gas) and vice versa, particle-particle collisions and particle-wall collisions. Additionally, a ray-tracing method, similar to the approach of Toschkoff et al. [6], is applied to model spray droplet deposition. Fluid phase equations are solved using the CFD code “AVL-Fire”, while for the particle motion and spray modelling the DEM code

"XPS" is used. For details on the coupling procedure, the reader is referred to [7].

The governing equations for the fluid phase are derived from the Navier-Stokes equations by considering local volume averaged quantities as typical for the unresolved CFD-DEM:

$$\frac{\partial}{\partial t}(\phi_f \rho_f) + \nabla(\phi_f \rho_f \boldsymbol{v}_f) = 0 \tag{1}$$

$$\begin{aligned}\frac{\partial}{\partial t}(\phi_f \rho_f \boldsymbol{v}_f) + \nabla \cdot (\phi_f \rho_f \boldsymbol{v}_f \boldsymbol{v}_f) \\ = -\nabla \cdot (\phi_f \tau_f) - \phi_f \nabla p \\ + \phi_f \rho_f \boldsymbol{g} \\ - \frac{1}{V_{cell}} \sum_i \beta V_{p,i} (\boldsymbol{v}_f - \boldsymbol{v}_{p,i})\end{aligned} \tag{2}$$

where ϕ_f is the local fluid volume fraction, ρ_f the fluid density and $\boldsymbol{v}_f$ the fluid velocity vector. $\boldsymbol{\tau}_f$ is the fluid stress tensor, p the pressure, $\boldsymbol{g}$ the gravitational acceleration, V_{cell} the volume of the grid cell, β the drag coefficient, and $V_{p,i}$ and $\boldsymbol{v}_{p,i}$ are, respectively, the volume and velocity of particle i. The fluid was treated as incompressible with constant density, and vapor transferred to the gas was neglected.

Eq. (1) is the continuity equation, which ensures fluid mass conservation. Eq. (2) is the fluid momentum equation, consisting of the following terms: The left-hand side represents the change of fluid momentum, the terms on the right-hand side account for viscous stress, the pressure field, gravitation, and the momentum transferred from the particle phase. The drag coefficient for momentum transfer between fluid and particle phase is calculated with the correlation of Beetstra et al. [8].

The particle movement is determined with Newton's translational and rotational equations of motion:

$$\rho_p V_p \frac{d\boldsymbol{v}_p}{dt} = \boldsymbol{f}_c + \rho_p V_p \boldsymbol{g} - V_p \nabla p + \beta V_p (\boldsymbol{v}_f - \boldsymbol{v}_p) \tag{3}$$

$$I_p \frac{d\boldsymbol{\omega}_p}{dt} = \boldsymbol{M}_p \tag{4}$$

where ρ_p is the particle density, V_p the particle volume, $\mathbf{v}_p$ the particle velocity, $\mathbf{f}_c$ the resultant of all particle-particle and particle-wall contact forces, $\mathbf{g}$ the gravitational acceleration, ∇p the pressure gradient, β the drag coefficient and $\mathbf{v}_f$ the fluid velocity. I_p is the moment of inertia, $\boldsymbol{\omega}_p$ the angular particle velocity and $\boldsymbol{M}_p$ the total torque acting on the particle.

In Eq. (3), the terms on the right hand side account for the particle-particle and particle-wall contact forces, the gravitational force, the pressure field and the momentum transfer from the fluid phase. The contact forces are calculated with a linear spring-dashpot model as used in Forgber et al. [9].

The simulations represent a Glatt GPCG-2 6" Wurster coater. The coating chamber has a height of 0.63 m and a diameter of 0.14 m and 0.3 m at the inlet and outlet, respectively. To reduce the computational effort, only a 90° section of the coater was simulated, using a symmetry (CFD) and frictionless wall (DEM) boundary condition. To obtain a torus-shaped flow inside the coater (particles travel upwards inside the Wurster tube and fall back down outside), the air inlet is controlled via different sized holes in the bottom plate. To reduce simulation time, the bottom plate is approximated by a porous layer. Similar to the different sized holes in the real bottom plate, the inlet boundary condition is split into four sections. The porosity of the sections in the plate is set to the area ratio of holes to total area, the massflow ratio is specified in Figure 2. Another inlet boundary condition (normal velocity of 75 m/s) is applied to the nozzle to account for the atomizing airflow. At the outlet, a static pressure of 1 atm is assumed. The timestep is 0.001 s for the CFD calculation and 5e-6 s for DEM. The particle size follows a truncated gaussian distribution in the range of 624 µm and 884 µm. The mean particle diameter is 754 µm with a standard deviation of 14 µm, the total solid mass in the quarter model is 0.323 kg, resulting in 0.991 Mio. particles. The parameters for the DEM simulation are given in Table 1.

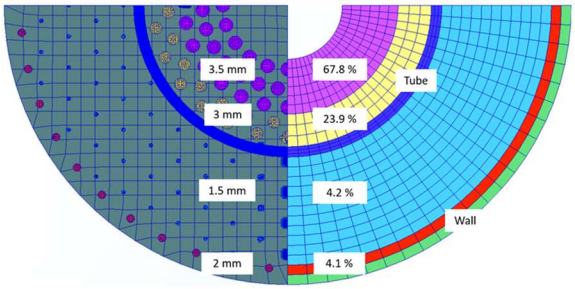

Figure 2: Mesh of the real bottom plate (left) and bottom plate model used in simulation (right). The values on the left are the diameters of the holes in the sections, on the right, the massflow through each section is specified.

Table 1: Parameters used for the DEM simulation.

Property	Unit	Value
Particle density	kg/m³	1420
Mean particle diameter	µm	754
Normal spring stiffness k	N/m	2000
Tangential spring stiffness	N/m	1600
Friction coefficient	-	0.05

Model Development

The proposed model is derived from a statistical approach developed by Mann [10]. This model is based on the principle that the amount of coating, which a single particle receives, depends on two factors: (i) how often the particle travels through the spray zone and (ii) how much coating is deposited during one spray zone visit (coating gain). Hence, the model parameters are the mean number of cycles during the whole coating process N_{cycles}, the cycle time (CT) variability and the coating gain (CG) variability:

$$CV_{total} = \sqrt{\frac{CV_{CT}^2 + CV_{CG}^2}{N_{cycles}}} \tag{5}$$

where CV_{total} is the coefficient of variation of the inter-particle coating mass, CV_{CT} is the coefficient of variation of the cycle time distribution, and CV_{CG} is the coefficient of variation of the coating gain distribution. The mean number of cycles can be calculated as

$$N_{cycles} = \frac{t_{coating}}{\mu_{CT}} = \frac{m_{coating}}{\dot{m}_{spray} \mu_{CT}} \tag{6}$$

$$m_{coating} = \frac{m_{batch} CL}{(1 - CL) x_{solid}} \tag{7}$$

where $t_{coating}$ is the total coating time, μ_{CT} is the mean cycle time, $m_{coating}$ is the mass of the spray solution, $\dot{m}_{spray}$ is the spray rate, m_{batc} is the initial batch mass, CL is the coating level and x_{solid} is the mass fraction of solid coating in the spray solution. The coating level is defined as

the ratio of coating mass to batch mass after the process, i.e. the mass fraction of solid coating in the final product:

$$CL = \frac{m_{solid}}{m_{batch} + m_{solid}} \quad (8)$$

where m_{solid} is the mass of the solid coating substance sprayed.

While the batch mass, the coating level, the mass fraction of solids in the spray solution and the spray rate are input parameters to the process, the mean cycle time, cycle time variability and coating gain variability can be extracted from the CFD-DEM simulations. The results for varying inlet airflow rates (70 – 90 m³/h) and spray rates (10 – 30 g/min) are given in Table 2 (coating level: 5%, solid mass fraction: 5%). With the results of the CFD-DEM simulation available, we can make three assumptions to simplify Eq. (5) to reduce the model.

1. $CV_{CT} \ll CV_{CG}$
   The investigations show, that the variations in cycle time are much smaller than the variations in coating gain. Hence, the cycle time variability can be neglected.
2. $CV_{CG} \approx const.$
   The variations in coating gain do not differ much across the investigated parameter space. It was observed, that the spray rate and inlet air flow rate have a roughly equal impact on the mean and the standard deviation of the coating gain distribution, so the coefficient of variation remains almost constant. Hence, we can use the mean variability to predict the coating uniformity.
3. $\mu_{CT} = f(\dot{V}_{in})$
   The inlet air flow rate is the only parameter varied in this study, which affects the mean cycle time. For higher inlet air flow rates, the cycle time decreases due to the higher particle velocities. According to Figure 3, there is a linear correlation between the mean cycle time and the inlet air flow rate. Hence, we can estimate the mean cycle time with the equation of the linear regression line given in Figure 3.

These assumptions are valid as long as all other input variables and process parameters remain unchanged, e.g. coater geometry (e.g. Wurster gap), batch mass or material properties. By applying the above assumptions to Eq. (5), the total coating variability can be estimated as

$$CV_{total} = \frac{\overline{CV}_{CG}}{\sqrt{N_{cycles}}} = \overline{CV}_{CG}\sqrt{\frac{\dot{m}_{spray}\mu_{CT}}{m_{coating}}} \quad (9)$$

$$\mu_{CT} = c_1\dot{V}_{in} + c_2 \quad (10)$$

where $\dot{V}_{in}$ is the inlet air flow rate and c_1 and c_2 are the fitting parameters of the linear regression.

Table 2: Results of the CFD-DEM simulation runs.

Run [-]	$\dot{V}_{in}$ [m³/h]	$\dot{m}_{spray}$ [g/min]	N_{cycles} [-]	CV_{CT} [%]	CV_{CG} [%]	CV_{total} [%]
1	70	20	1558	15.5	733.8	18.6
2	80	20	1682	14.1	729.8	17.8
3	90	20	1860	13.9	735.4	17.1
4	80	10	3369	14.1	729.2	12.6
5	80	30	1123	14.2	725.5	21.7

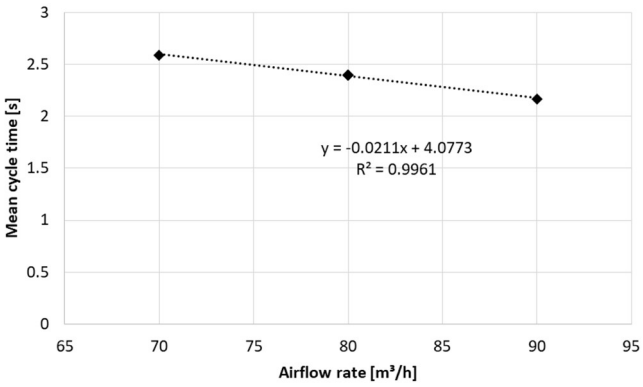

Figure 3: Linear regression of inlet air flow rate and mean cycle time.

Validation

To ensure the validity of the simplified coating model, additional CFD-DEM simulations were carried out. For a total of 16 runs with different input parameters, the results of the base model (Eq. (5)) are compared with the simplified version (Eq. (8)). Table 3 provides an overview over the validation runs. The inlet air flow rate varies between 70 and 90 m³/h, the spray rate between 10 and 30 g/min and both the coating level and the solid mass fraction (in the coating) between 3 and 7%. The results of the validation runs are presented in Figure 4. With observed mean and maximum relative errors of 0.51 and 0.76% respectively, the reduced model proves the ability to correctly predict the coating variability across the whole operating space. This also justifies the assumptions made above to distill the coating model, which does not require additional simulations or measurements.

As every model, the presented approach comes along with some limitations. Since statistical models are not based on the underlying physical phenomena, they are not flexible with regard to process parameters. The coating model is only valid if all process parameters (except the input parameters to the model) are kept constant. Furthermore, the statistics obtained from the CFD-DEM simulations were evaluated for the whole particle bed. No differences in particle size or other material properties were considered, although it is known that the cycle time is affected by the particle size distribution (PSD) [11]. Hence, the approach is valid for raw particles with a comparably narrow PSD only.

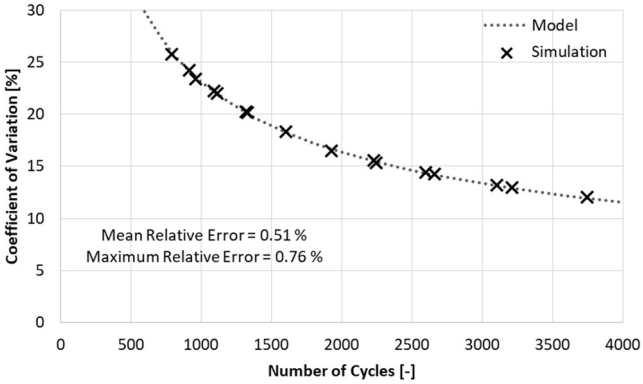

Figure 4: Comparison of simulation results with the simplified statistical model.

Table 3: Parameters for the model validation runs.

Run [-]	$\dot{V}_{in}$ [m³/h]	$\dot{m}_{spray}$ [g/min]	CL [%]	x_{solid} [%]
1	70	20	5	3
2			5	7

3			3	5
4			7	5
5			5	3
6		15	5	7
7			3	5
8	80		7	5
9			5	3
10		25	5	7
11			3	5
12			7	5
13			5	3
14	90	20	5	7
15			3	5
16			7	5

Discussion

By examining Eq. (9), favorable process conditions in terms of coating uniformity can be derived. The coating variability scales with the inverse square root of the number of cycles, which in turn depends on the coating time and the mean cycle time (Eq. (7)). As mentioned before, the cycle time decreases with increasing air flow rate. Therefore, higher inlet air flow rates are beneficial for the coating uniformity. On the other hand, the coating time is a function of the spray rate, the coating level and the solid mass fraction. It is well known, that the coating uniformity increases for longer process run times [12]. However, from an economical point of view, short coating times are desirable. Hence, the coating time should be as small as possible, but still long enough to obtain the desired product quality.

A simple way to increase the coating time is reducing the spray rate. Unfortunately, lower spray rates also reduce the coating yield because of higher spray drying losses [13]. Spray drying is the effect of droplets drying before colliding with a particle. The risk of spray drying increases, if volatile organic compounds are used as spray solution. Dried out droplets are not deposited on particles due to the missing binding liquid and are collected in the filters at the outlet of the coating device. High coating yields are especially desirable for active coating layers, in which an Active Pharmaceutical Ingredient (API) is applied to inert core beads.

The second approach to increase the coating time would be increasing the coating level. This means that the coating mass per particle increases, causing higher coating thickness too. Such a method is only feasible for coatings, which do not affect the effectiveness of the drug, e.g. sugar coatings. For active coating layers or modified release coatings, the coating level is predetermined to achieve the desired drug performance.

The third parameter affecting the coating time is the solid mass fraction in the spray solution. With the solid content, the spray viscosity, spreading behavior of the deposited droplet and film formation might change. However, it seems to be a good alternative to control the coating time if the coating level cannot be adjusted.

Another way to reduce the coating variability is by reducing the coating gain variability. This could be achieved by optimizing the particle flow through the Wurster tube. The parameters investigated did not have significant impact on the coating gain variability. However, it is known that the Wurster gap height, or the airflow distribution through the bottom plate are of relevance [14]. Unfortunately, optimizing those parameters is a difficult task, since it is hardly possible to obtain the coating gain distribution experimentally. For that purpose, CFD-DEM simulations could provide valuable information.

Finally, the coating gain variability could be reduced by the adjusting the droplet size. An increased number of droplets potentially leads to a better spray distribution. The droplet size can be regulated via the nozzle geometry and the atomizing air pressure. However, similar to the spray rate, small droplets lead to increased spray drying, limiting the coating yield.

Concluding the above, selecting process parameters for the Wurster coating process is always a tradeoff between quality and efficiency. Additionally, it is difficult to capture some of the most critical aspects experimentally. This highlights the need for sophisticated modeling approaches. While CFD-DEM simulations provide detailed insight to the physical phenomena during the process, statistical models like the one presented in this work are essential for successful process design.

Outlook

While the proposed model can help to determine the coating variability of a Wurster coating process, it does not provide flexibility regarding to some relevant process parameters. With additional CFD-DEM simulations, the effect of the Wurster gap height and the batch mass could be investigated to adjust the model accordingly. Furthermore, one could try to capture the effect of different particle sizes on the coating distribution. For the CFD-DEM model, heat and mass transfer may be added to predict the coating losses arising from spray drying.

Acknowledgement

RCPE is a K1 COMET Centre within the COMET – Competence Centres for Excellent Technologies programme. The COMET programme is operated by the Austrian Research Promotion Agency (FFG) on behalf of the Federal Ministry for Transport, Innovation and Technology (BMVIT) and the Federal Ministry for Digital and Economic Affairs (BMDW). Our projects are also funded by Land Steiermark and the Styrian Business Development Agency (SFG).

References

[1] L. Fries, S. Antonyuk, S. Heinrich, and S. Palzer, “DEM-CFD modeling of a fluidized bed spray granulator,” *Chem. Eng. Sci.*, vol. 66, no. 11, pp. 2340–2355, 2011, doi: 10.1016/j.ces.2011.02.038.

[2] M. Askarishahi, M.-S. Salehi, and S. Radl, “Full-Physics Simulations of Spray-Particle Interaction in a Bubbling Fluidized Bed,” *AIChE J.*, vol. 63, no. 7, pp. 2569–2587, 2017, doi: 10.1002/aic.15616.

[3] A. Sarkar *et al.*, “Multiscale Modeling of a Pharmaceutical Fluid Bed Coating Process using CFD/DEM and Population Balance Models to Predict Coating Uniformity,” in *Chemical Engineering in the Pharmaceutical Industry*, 2nd ed., 2019, pp. 419–450.

[4] P. Kieckhefen, T. Lichtenegger, S. Pietsch, S. Pirker, and S. Heinrich, “Simulation of Spray Coating in a Spouted Bed using Recurrence CFD,” *Particuology*, vol. 42, pp. 92–103, 2019, doi: 10.1016/j.partic.2018.01.008.

[5] Z. Jiang, C. Rieck, A. Bück, and E. Tsotsas, “Modeling of inter- and intra-particle coating uniformity in a Wurster fluidized bed by a coupled CFD-DEM-Monte Carlo approach,” *Chem. Eng. Sci.*, vol. 211, 2020, doi: 10.1016/j.ces.2019.115289.

[6] G. Toschkoff *et al.*, “Spray models for discrete element simulations of particle coating processes,” *Chem. Eng. Sci.*, vol. 101, pp. 603–614, 2013, doi: 10.1016/j.ces.2013.06.051.

[7] D. Jajcevic, E. Siegmann, C. Radeke, and J. G. Khinast, “Large-scale CFD–DEM simulations of fluidized

granular systems," *Chem. Eng. Sci.*, vol. 98, pp. 298–310, 2013, doi: 10.1016/J.CES.2013.05.014.

[8] R. Beetstra, M. A. Van Der Hoef, and J. A. M. Kuipers, "Drag Force of Intermediate Reynolds Number Flow Past Mono- and Bidisperse Arrays of Spheres," *AIChE J.*, vol. 53, no. 2, pp. 489–501, 2007, doi: 10.1002/aic.

[9] T. Forgber, P. Toson, S. Madlmeir, H. Kureck, J. G. Khinast, and D. Jajcevic, "Extended validation and verification of XPS/AVL-Fire™, a computational CFD-DEM software platform," *Powder Technol.*, vol. 361, pp. 880–893, 2020, doi: 10.1016/J.POWTEC.2019.11.008.

[10] U. Mann, "Analysis of Spouted-Bed Coating and Granulation. 1. Batch Operation," *Ind. Eng. Chem. Process Des. Dev.*, vol. 22, no. 2, pp. 288–292, 1983, doi: 10.1021/i200021a019.

[11] P. Böhling *et al.*, "Computational Fluid Dynamics-Discrete Element Method Modeling of an Industrial-Scale Wurster Coater," *J. Pharm. Sci.*, vol. 108, pp. 538–550, 2019, doi: 10.1016/J.XPHS.2018.10.016.

[12] R. Turton, "Challenges in the modeling and prediction of coating of pharmaceutical dosage forms," *Powder Technol.*, vol. 181, no. 2, pp. 186–194, 2008, doi: 10.1016/j.powtec.2006.12.006.

[13] A. van Kampen and R. Kohlus, "Statistical modelling of coating layer thickness distributions: Influence of overspray on coating quality," *Powder Technol.*, vol. 325, pp. 557–567, 2018, doi: 10.1016/j.powtec.2017.11.031.

[14] D. Jones and E. Godek, *Development, optimization, and scale-up of process parameters: Wurster coating*. Elsevier Inc., 2016.